

---

---

**Space environment (natural and artificial) — Procedure for obtaining worst case and confidence level of fluence using the quasi-dynamic model of earth's radiation belts**

*Environnement spatial (naturel et artificiel) — Mode opératoire pour obtenir le cas le plus défavorable et le niveau de confiance de la fluence en utilisant le modèle quasi-dynamique des ceintures de radiation terrestres*

STANDARDSISO.COM : Click to view the PDF of ISO/TS 21979:2018



STANDARDSISO.COM : Click to view the full PDF of ISO/TS 21979:2018



**COPYRIGHT PROTECTED DOCUMENT**

© ISO 2018

All rights reserved. Unless otherwise specified, or required in the context of its implementation, no part of this publication may be reproduced or utilized otherwise in any form or by any means, electronic or mechanical, including photocopying, or posting on the internet or an intranet, without prior written permission. Permission can be requested from either ISO at the address below or ISO's member body in the country of the requester.

ISO copyright office  
CP 401 • Ch. de Blandonnet 8  
CH-1214 Vernier, Geneva  
Phone: +41 22 749 01 11  
Fax: +41 22 749 09 47  
Email: [copyright@iso.org](mailto:copyright@iso.org)  
Website: [www.iso.org](http://www.iso.org)

Published in Switzerland

# Contents

	Page
Foreword .....	iv
Introduction .....	v
<b>1 Scope .....</b>	<b>1</b>
<b>2 Normative references .....</b>	<b>1</b>
<b>3 Terms and definitions .....</b>	<b>1</b>
<b>4 Radiation belts model .....</b>	<b>2</b>
<b>5 Principles of the method .....</b>	<b>3</b>
5.1 Cumulative fluence .....	3
5.2 Confidence level .....	3
5.3 Quasi-dynamic model of Earth's radiation belts .....	3
5.3.1 Overview .....	3
5.3.2 Available models .....	3
5.4 Remarks .....	3
<b>Annex A (informative) .....</b>	<b>4</b>
<b>Annex B (informative) CRRESELE Model .....</b>	<b>7</b>
<b>Annex C (informative) MDS-1 Radiation Belt Model .....</b>	<b>8</b>
<b>Bibliography .....</b>	<b>18</b>

## Foreword

ISO (the International Organization for Standardization) is a worldwide federation of national standards bodies (ISO member bodies). The work of preparing International Standards is normally carried out through ISO technical committees. Each member body interested in a subject for which a technical committee has been established has the right to be represented on that committee. International organizations, governmental and non-governmental, in liaison with ISO, also take part in the work. ISO collaborates closely with the International Electrotechnical Commission (IEC) on all matters of electrotechnical standardization.

The procedures used to develop this document and those intended for its further maintenance are described in the ISO/IEC Directives, Part 1. In particular, the different approval criteria needed for the different types of ISO documents should be noted. This document was drafted in accordance with the editorial rules of the ISO/IEC Directives, Part 2 (see [www.iso.org/directives](http://www.iso.org/directives)).

Attention is drawn to the possibility that some of the elements of this document may be the subject of patent rights. ISO shall not be held responsible for identifying any or all such patent rights. Details of any patent rights identified during the development of the document will be in the Introduction and/or on the ISO list of patent declarations received (see [www.iso.org/patents](http://www.iso.org/patents)).

Any trade name used in this document is information given for the convenience of users and does not constitute an endorsement.

For an explanation of the voluntary nature of standards, the meaning of ISO specific terms and expressions related to conformity assessment, as well as information about ISO's adherence to the World Trade Organization (WTO) principles in the Technical Barriers to Trade (TBT) see [www.iso.org/iso/foreword.html](http://www.iso.org/iso/foreword.html).

This document was prepared by Technical Committee ISO/TC 20, *Aircraft and space vehicles*, Subcommittee SC 14, *Space systems and operations*.

Any feedback or questions on this document should be directed to the user's national standards body. A complete listing of these bodies can be found at [www.iso.org/members.html](http://www.iso.org/members.html).

## Introduction

The space environment changes greatly due to solar activity, magnetic storms, etc. Therefore, the radiation fluence environment received by a satellite varies depending on its launch date, orbit, and operation period.

What is important for satellite design is the worst condition and confidence level of fluence. Optimum design can be done by knowing these conditions. Although the radiation belts model so far can be distinguished between the solar activity maximum and the minimum, it was difficult to deal with short-term and long-term fluctuations. The procedure for obtaining the worst condition and confidence level of fluence is defined using the quasi-dynamic model of Earth's radiation belts.

STANDARDSISO.COM : Click to view the full PDF of ISO/TS 21979:2018

STANDARDSISO.COM : Click to view the full PDF of ISO/TS 21979:2018

# Space environment (natural and artificial) — Procedure for obtaining worst case and confidence level of fluence using the quasi-dynamic model of earth's radiation belts

## 1 Scope

This document, by using a model that reproduces the fluctuations of radiation belts, defines the calculation method (orbit, operation period) of the radiation fluence received by a satellite. The quasi-dynamic model of Earth's radiation belts adopts input parameters (index values) to predict variation. The input parameters are selected from those that are easy to obtain data and have high correlation with the variation in Earth's radiation belts.

NOTE This method is an engineering method used for satellite design and similar purposes.

## 2 Normative references

There are no normative references in this document.

## 3 Terms and definitions

For the purposes of this document, the following terms and definitions apply.

ISO and IEC maintain terminological databases for use in standardization at the following addresses:

- ISO Online browsing platform: available at <https://www.iso.org/obp>
- IEC Electropedia: available at <https://www.electropedia.org/>

### 3.1

#### **L-value**

distance to a point where the magnetic lines of force intersect with the equatorial plane of the geomagnetic field from Earth's core, with  $R_e$  (radius of Earth) used as the unit

### 3.2

#### **B/B<sub>0</sub>**

value normalized to the minimum value of the field line in the magnetic equator

### 3.3

#### **K<sub>p</sub> and a<sub>p</sub>**

planetary indices that are based on 3-hour measurements from 13 ground stations

Note 1 to entry: Values of  $a_p$  range from 0 to 400 and are expressed in units of 2 nT.  $K_p$  is essentially the logarithm of  $a_p$ , with its scale of 0 to 9 being expressed in thirds of a unit (e.g., 5- = 4 2/3, 5<sub>0</sub> = 5, 5+ = 5 1/3). A daily index ( $A_p$ ) is obtained by averaging the eight values of  $a_p$  for each day and the index  $A_p$  can have values intermediate to those of  $a_p$

### 3.4

#### **solar wind speed**

outward flux of solar particles and magnetic fields from the Sun used in external magnetic field model computation

Note 1 to entry: Typically, solar wind velocities are around 350 km/s-1.

### 3.5

#### **F10.7**

F10

traditional solar energy proxy that is used on atmosphere models

Note 1 to entry: Measure of the solar radio flux at a wavelength of 10,7 cm at Earth's orbit, given in units of 10–22 W·m–2.

### 3.6

#### **Sunspot number**

**R**

Ri

Rz

daily index of sunspot activity, defined as  $R=k(10g+s)$  where  $s$  is the number of individual spots,  $g$  the number of sunspot groups, and  $k$  is an observatory factor

[SOURCE: ISO 16457:2014, modified — synonymous terms editorially revised for alignment with ISO/IEC Directives Part 2]

### 3.7

#### **Dst**

##### **Disturbance storm time**

geomagnetic index used in external magnetic field model computation that describes variations in the equatorial ring current and is derived from hourly scalings of low-latitude horizontal magnetic variation

Note 1 to entry: Dst is expressed in nT.

### 3.8

#### **IMF**

##### **Interplanetary Magnetic Field**

geomagnetic index used in external magnetic field model computation that corresponds to the part of the Sun's magnetic field that is carried into interplanetary space by solar wind

Note 1 to entry: The three orthogonal components of the IMF are  $B_x$ ,  $B_y$ , and  $B_z$ .  $B_x$  and  $B_y$  are oriented parallel to the ecliptic.

Note 2 to entry: The IMF is a weak field, varying in strength near Earth from 1 to 37 nT, with an average of about 6 nT.

## 4 Radiation belts model

The magnetically trapped radiation around Earth is known as the Van Allen belts. The belts consist of energetic electrons from ~100 keV to 10 s of MeV and protons from ~100 keV up to around 1 GeV. The belts are organized into an inner zone and an outer zone separated by a slot region. Below 100 keV, a plasma population, known as the ring current, is also magnetically confined in this region.

Currently, many of the models used in satellite design are what we call a static model to predict the average particle distribution. However, the actual environment from various observation data fluctuates much more complexly than the static environment described by their models. In particular, spatial and especially temporal variations in satellite design are becoming more important than previously believed. When designing a satellite, the uncertainty of these models is dealt with by taking a design margin. Currently, physics-based models that enable an understanding and prediction of the dynamics of Earth's radiation belts are now available, but are complicated models that require a lot of parameter data. However, there is also a simple quasi-dynamic model of Earth's belts that predicts variations in the radiation belts with several input parameters (highly available, long-term accumulated index). This document specifies the worst case and confidence level calculation method using the latter model.



## 5 Principles of the method

### 5.1 Cumulative fluence

See ISO 12208:2015, 4.1.

### 5.2 Confidence level

See ISO 12208:2015, 4.2.

### 5.3 Quasi-dynamic model of Earth's radiation belts

#### 5.3.1 Overview

The variations in radiation belt particles greatly depending on the solar cycle effect, secular changes in the geomagnetic field, the anisotropy of trapping, and the geomagnetic state. The variations of the radiation belts can be predicted quasi-empirically by using the activity level of the Sun and disturbance of the geomagnetic field. Most activity indices are given for short periods and as long duration averages. By statistically analysing the variations of these indices and radiation belts, it is possible to predict variations of radiation belts quasi-empirically. The input parameters are selected from those that are easy to obtain data and have high correlation with Earth's radiation belt variations.

The solar activity indices include Sunspot number (R), F10.7, solar wind speed, and so on. Also, Kp and ap, Dst and IMF are examples of geomagnetic activity indices.

[Annex A](#) shows the procedure for calculating the worst case and reliability level using the quasi-dynamic model.

#### 5.3.2 Available models

- a) CRRESSELE model in [Annex B](#).
- b) MDS-1 Radiation belt model in [Annex C](#).

### 5.4 Remarks

- a) The worst case and confidence level of fluence can be easily obtained by using the radiation belts variation parameter SW, AP, and F10.7 index.
- b) This technique is applicable when there are at least ten years' worth of parameters used to predict radiation belt fluctuation.
- c) Although the design margin has thus far been left to the judgment of the satellite designer, it is possible to set the margin accurately from the worst environment.

## Annex A (informative)

### A.1 Procedure for obtaining worst case and confidence level of fluence using the quasi-dynamic model of Earth's radiation belts

Select the dynamic model of Earth's radiation belts. The probability distribution of one-day radiation fluence operation is calculated by assuming that the satellite was launched on one day in the past and started its operation. The radiation fluence is calculated by changing the day of the launch and a histogram is created to obtain the probability of the radiation fluence. The detailed calculation method is described as follows. Estimate cumulative fluence by using the method in [5.1](#) Cumulative fluence.

1) Calculation of the orbital position (B/B0-L)

The number of days longer than the recurrence period, here 30 days is used as an example, is used for a low-orbit satellite to minimize the effect of the orbital position on the variation of radiation. The orbital positions during 30 days after the predetermined day of the launch are calculated and converted to B/B0-L.

2) Calculation of daily average particle fluence

The particle fluence is calculated for each 30-day period by changing the date one day at a time from the past to the present (during this period the driving parameters are known) using B/B0-L obtained in 1). The daily average particle fluence is calculated from the particle fluence over 30 days.

3) Calculation of fluence during operation

The fluence during operation is calculated by assuming that the daily average particle fluence obtained in 2) is the one-day particle fluence and accumulating the one-day particle fluences for an arbitrary operation period by delaying the operation start date one day at a time from the past to the present.

4) Calculation of the maximum, minimum, and average fluences during operation

The maximum and minimum fluence are determined from the results obtained in 3), and the average fluence is calculated.

5) Creation of a histogram

A histogram of the fluence during operation is created using the results obtained in 4).

6) Probability distribution

The probability of occurrence of fluence during operation is calculated using histogram obtained in 5).

Then, a reliability curve is obtained in the form of a probability distribution.

[Table A.1](#) summarizes the calculation conditions used in the example. In this example, a reliability curve for the fluence of a day during operation is obtained by the calculation of fluence between 1984 and 2010. [Figure A.1](#) shows the one-day particle fluence for different days of launch. In this example, the maximum fluence was on 1 November 2003. This may be because many large magnetic storms were

generated in 2003. Figure A.2 shows the confidence level curves obtained using the AE8 radiation belt model and the dynamic model of Earth's radiation belts.

**Table A.1 — Model Usage Example**

Item	Specification
Epoch	2009/12/31 21:10:45
Semi-major axis	7 047,049 427 km
Eccentricity	0,000 064 6
Inclination	98,070 3°
Right ascension of ascending node	112,118 8°
Argument of perigee	80,241 0°
Mean anomaly	279,888 4°

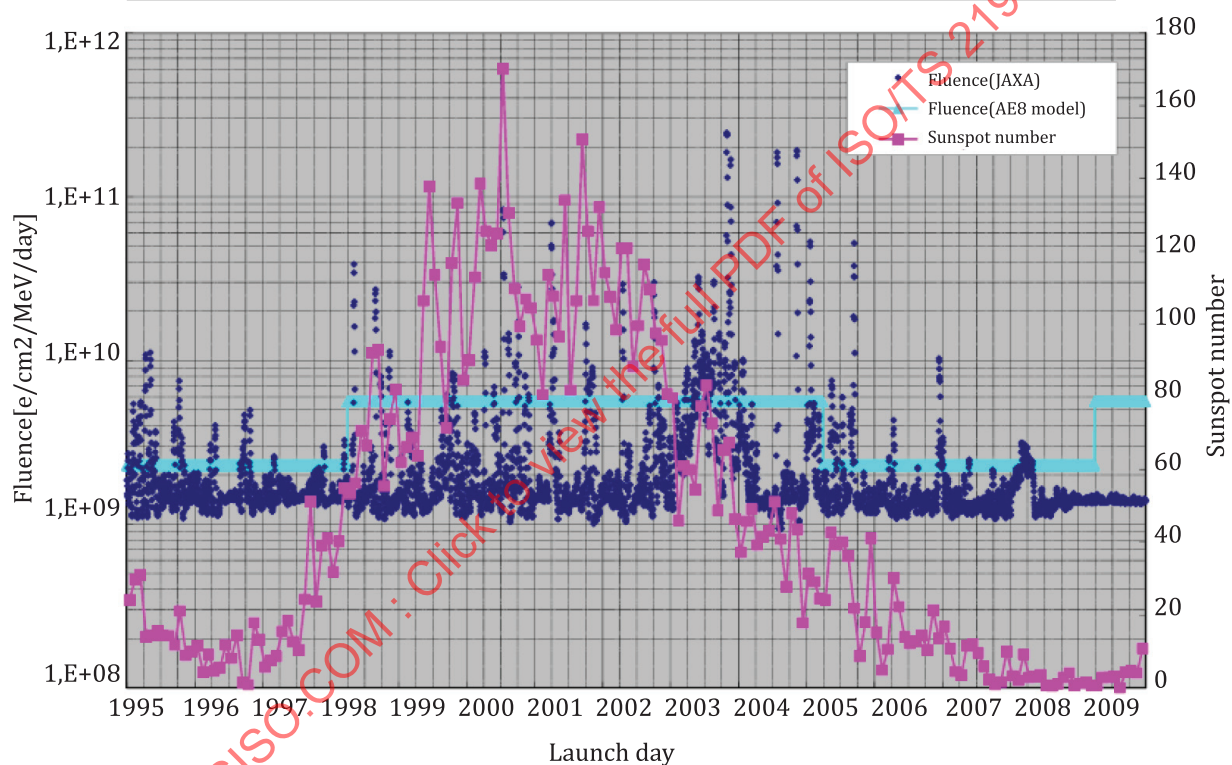


**Figure A.1 — Calculation process for daily average particle fluence (where the calculation start year is 1984)**

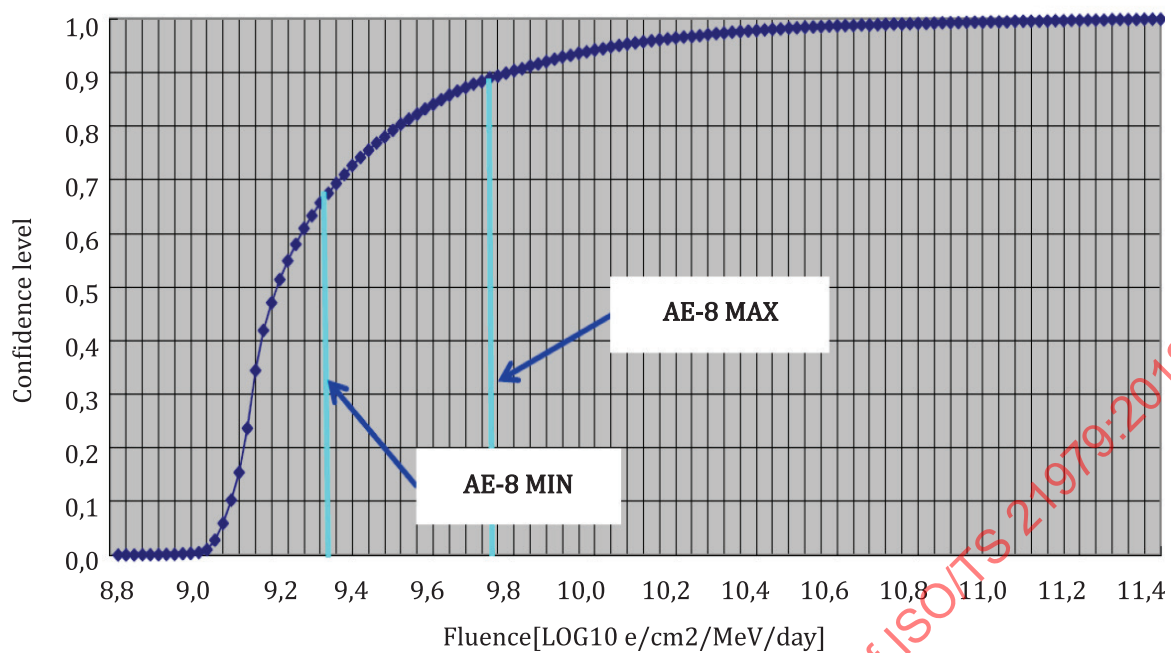
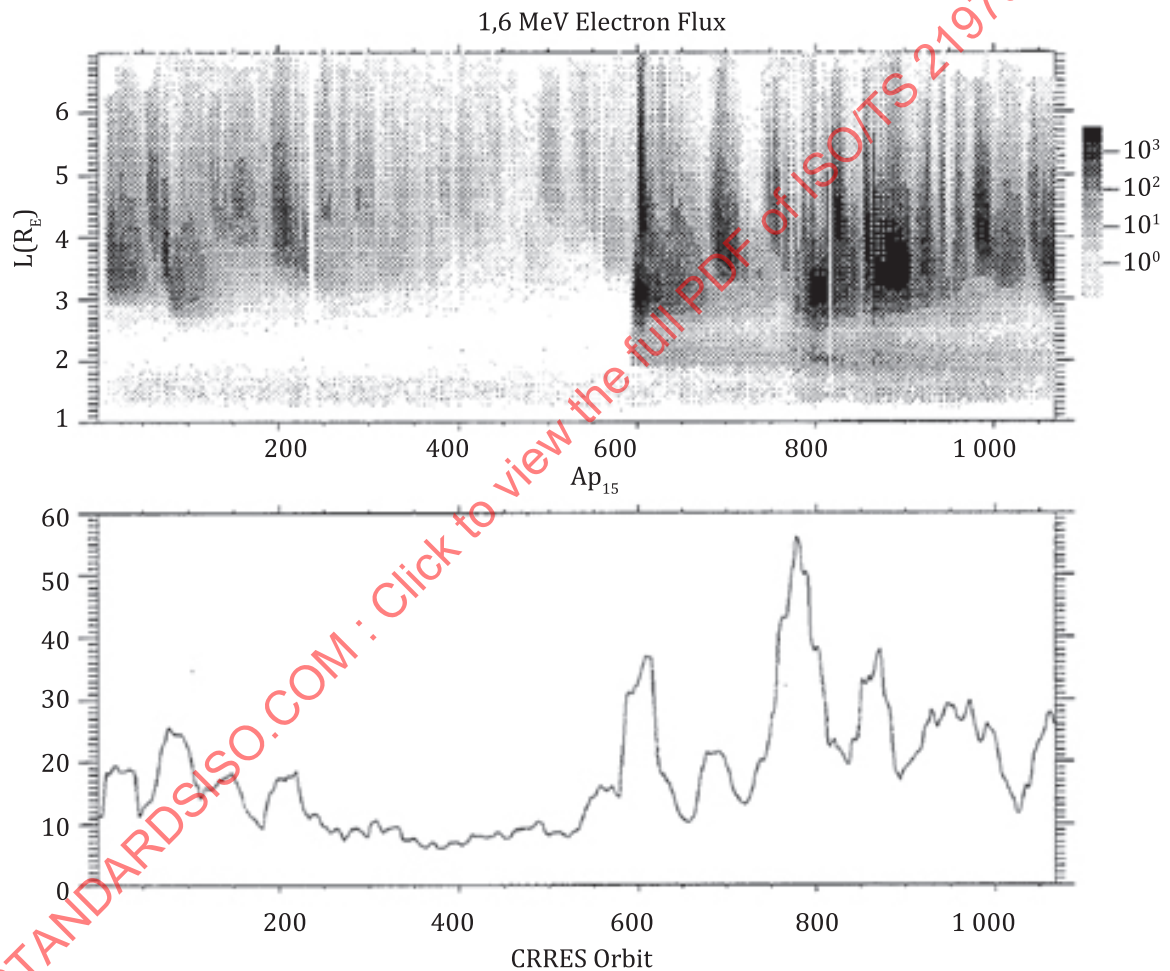


Figure A.2 — Confidence level for one-day fluence for electrons (0,4 - 0,9 MeV)

## Annex B (informative)

### CRRESELE Model

Data from the CRRES satellite in a geostationary transfer orbit (GTO) were used to build a number of models for the entire outer radiation belt zone under different geomagnetic activity conditions which are known as CRRESELE models<sup>[1]</sup>.  $Ap_{15}$ , the 15-day average of  $Ap$ , was used as a sorting parameter and it shows that generally the model fluxes increase over the entire outer belt with  $Ap_{15}$ . In these models, the same dependence on  $Ap_{15}$  is used for all L-values.



**Figure B.1 — Top panel: mission survey of 1,6 MeV electron flux in electrons/(cm<sup>2</sup> s sr keV) plotted for L sell versus CRRESS's orbit number. Bottom panel:  $Ap_{15}$  over the same period**

## Annex C (informative)

### MDS-1 Radiation Belt Model

#### C.1 Overview

The MDS-1 radiation belt model<sup>[2]</sup> was developed based on data from the MDS-1 spacecraft. Table C.1 shows a summary of the orbit of MDS-1, the data of which was used to develop the quasi-dynamic radiation belt model, and the specifications of the radiation-measuring system mounted on MDS-1. The sensor consists of three solid-state detectors (SSDs), a plastic scintillator, an anti-scintillator, and four photomultipliers. Low-energy cosmic radiation particles are detected by the SSDs. The amount of energy is measured from the amount of charge generated in the SSDs upon the incidence of particles. High-energy cosmic radiation particles pass through the SSDs and are detected by the scintillator located behind the SSDs. The light is converted into an electric signal in the photomultipliers to measure the amount of energy because the amount of luminance in the scintillator is proportional to the amount of energy. The peaks of the pulse waves generated in the SSDs and in the scintillator differ depending on type of incident particle and its energy. It is possible to determine the particles by coupling the SSDs and the scintillator. The energy resolution of the scintillator is inferior to that of the SSDs; however, the scintillator can be used to measure the amount of energy of high-energy electrons. The quasi-dynamic radiation belt model can cover the range of  $1,1 \leq L \leq 10$  ( $L$  is the multiple of Earth's radius) and  $1 \leq B/B_0 \leq 8,4$  ( $B$  and  $B_0$  are the magnetic fields at the geomagnetic equator, respectively) using the data collected by MDS-1.

**Table C.1 — MDS-1 Orbit and Specifications of Radiation-Measuring System Mounted on MDS-1**

Item	Specification
Inclination	$28,5^\circ$ , $1,1 \leq L \leq 10$
Altitude	$500 \text{ km} \times 36,000 \text{ km}$ , $1,1 \leq B/B_0 \leq 8,4$
Periods	About 10 hours, 35 minutes
Spin rate	5 rpm
Electron	0,4 - 9 MeV (5 bins)
Proton	0,9 - 210 MeV (12 bins)
He ion	6 - 140 MeV (4 bins)
Heavy ion	1,5 - 60 MeV/nuc (1 bin)
G-Factor	$0,01 \text{ cm}^2\text{sr}$

#### C.2 Definition of $T_{\text{avg}}$

Figure C.1 shows the variation of the energy of electrons (0,65 MeV) measured by MDS-1. The average log flux on an orbit from the apogee to the perigee is presented in colour for each orbit with an interval of  $L = 0,1 \text{ Re}$ . A radiation belt that significantly changes within a short period of time as shown in Figure C.1 cannot be classified into only two cases of solar minimum and maximum conditions as in the conventional model (AE8/AP8 radiation belt models). In this model, the radiation belt flux variation can be predicted by the following day using the average magnetic planetary (Ap) index representing the geomagnetic activity, solar wind speed, and F10.7 index as the driving parameters.

The variable parameter  $T_{\text{avg}}$  is used to predict the flux. It was confirmed that the predicted flux level for the following day, i.e.,  $\log [f(t, L)]$ , has a high correlation with the average of the variable parameters during  $T$  days before the date of prediction. Figure C.2 shows the definition of  $T_{\text{avg}}$ .



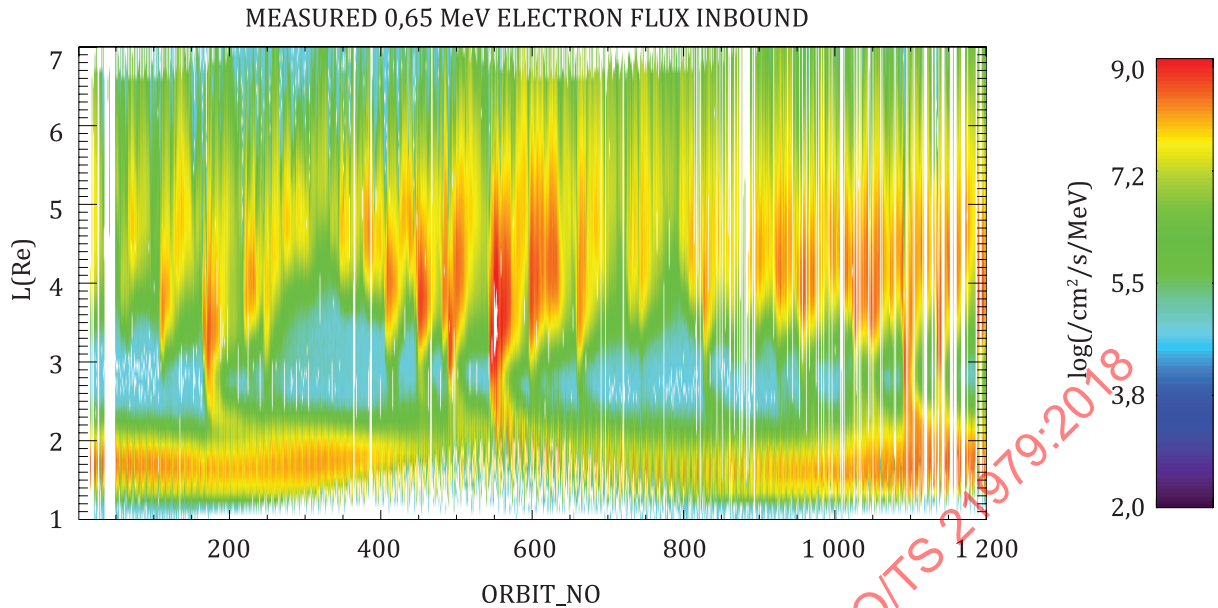


**Figure C.1 — Variation of electron energy observed by MDS-1 (where energy width of the bin is 0,35 to 0,78 MeV and the mean value is 0,65 MeV)**

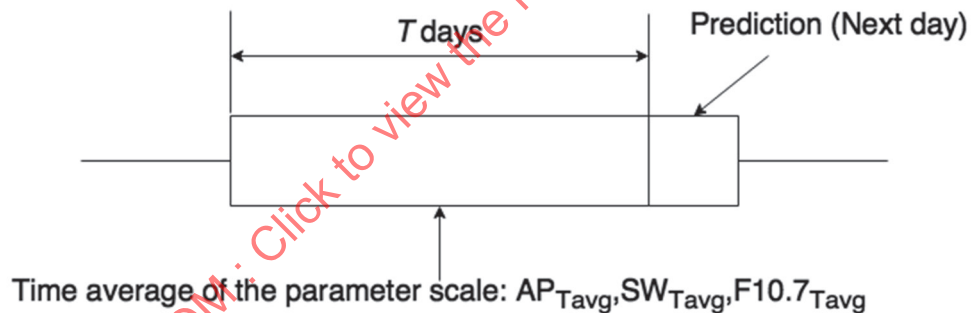


**Figure C.2 — Definition of  $T_{avg}$**

### C.3 Variation of radiation belt with Ap index, solar wind velocity, and F10.7 index

Figure C.3 shows the relationship of electron flux (0,4 - 0,9 MeV) with  $T_{avg}$  values, the Ap index, and solar wind velocity. The time average value with a high correlation coefficient for each L-value is indicated by a black dot.

The electron flux (0,4 - 0,9 MeV) in the inner belt has a high correlation with the Ap index and solar wind speed when  $T = 27$  (27 avg. values). This indicates the possibility that the inner belt varies as a result of the long-term variation in solar activity because 27 days correspond to the period of the Sun's rotation. In addition, the electron flux in the outer belt has a reasonable correlation with solar wind velocity in the vicinity of the geostationary orbit; however, the effect of the geomagnetic activity increases with decreasing L in other regions.

The variations of electron and proton fluxes have complicated relationships with the L-value and driving parameters (i.e., Ap index, solar wind speed, F10.7 index). In the model, the relative effects of these input parameters on the variations of electron and proton fluxes are taken into consideration.

Figure C.4 shows the relative effects of the solar wind velocity on the variation of electron flux (0,4 - 0,9 MeV).

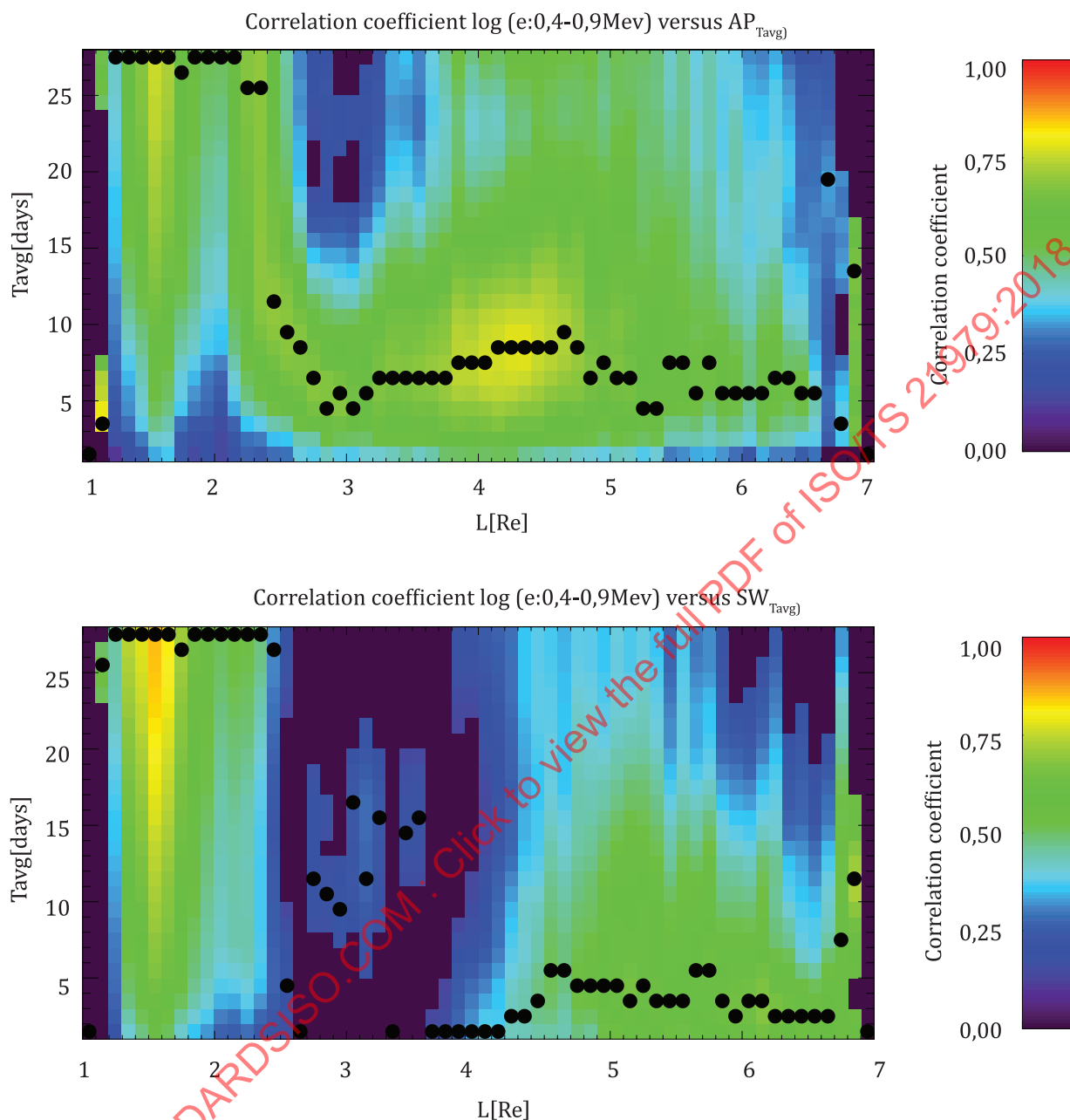
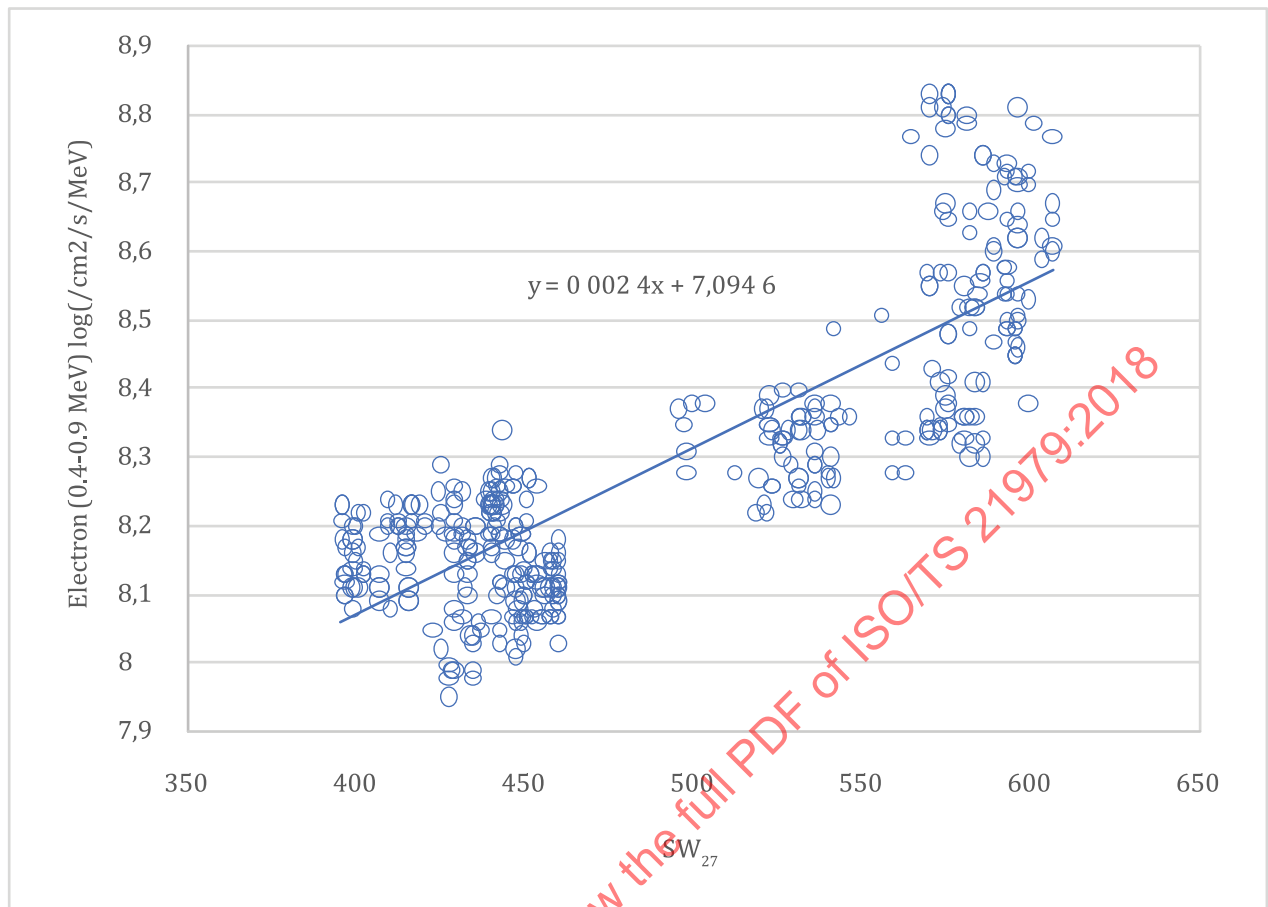


Figure C.3 — Relationship of electron flux (0,4 - 0,9 MeV)





**Figure C.4 — Relative effects of solar wind velocity on variation of electron flux (0,4 - 0,9 MeV) (where L-value is 1,6 Re in the case of the magnetic equator)**

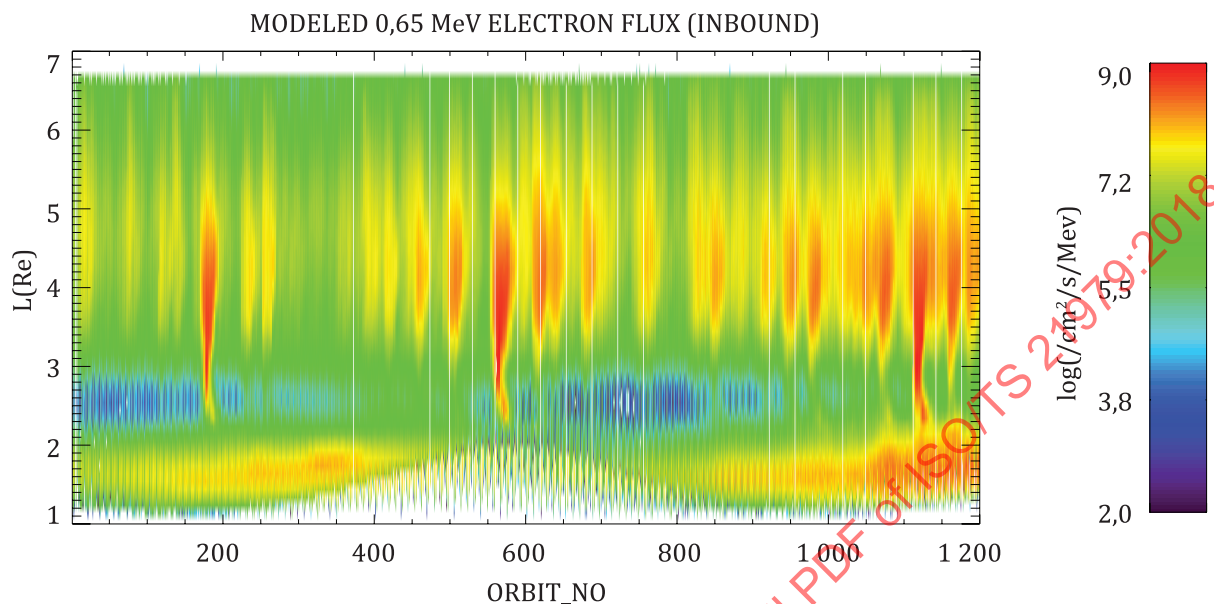
#### C.4 Overall structure of software

The input parameters for the developed software are the calculation duration (start time, end time), the six elements of the satellite orbit, the type of particles (electron, proton, He ion), the particle energy, the target information (omnidirectional fluence; the position, direction, and shape of radiation particles to determine the fluence),  $T_{avg}$  values of the Ap index, solar wind velocity, and F10.7 index. Using these parameters, omnidirectional fluence and unidirectional fluence considering various viewing angles are determined.

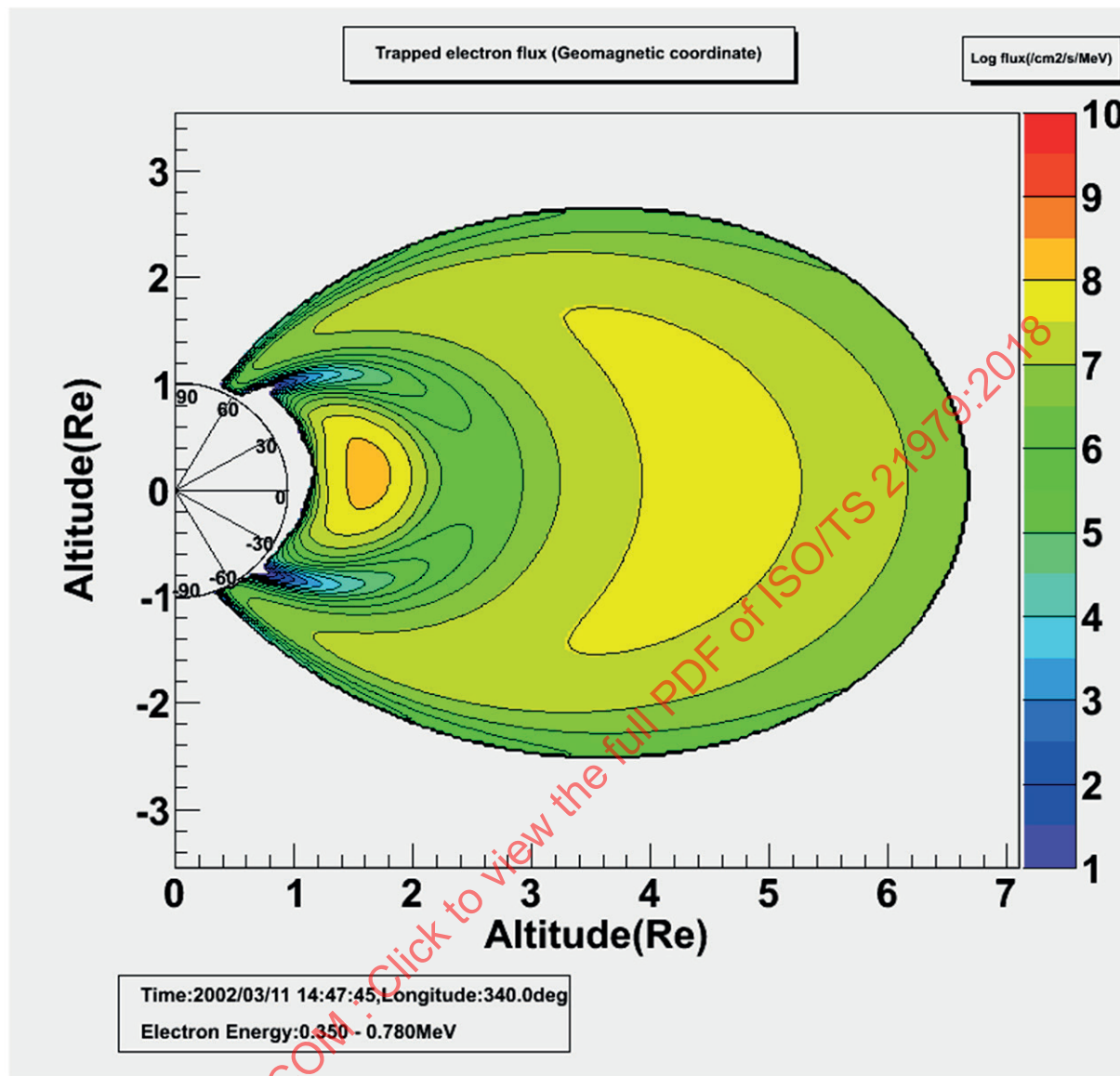
The L-value,  $B/B_0$ , and pitch angle ( $\alpha$ ) at each time are determined using the calculation duration, the six elements of the satellite orbit, the calculation interval, and the target information. The number of days ( $T_{avg}$ ) used for calculation is determined from the type of particle, the energy, and the L-value. From these results, the flux of  $B$  is determined as follows: (1) omnidirectional flux at the geomagnetic equator (magnetic field,  $B_0$ ) and (2) exponential coefficient  $n$  (used in the case of fitting with  $\sin^n \alpha$ ) are determined. Also, (3) the flux for conditions other than those at the geomagnetic equator (magnetic field,  $B$ ) is determined from the relationship between  $B/B_0$  and the omnidirectional flux, and (4)  $n$  is determined with respect to  $B$  from the relationship between  $B/B_0$  and  $n$ . For the calculations in (2) and (4), the results obtained by the analysis of measured data and an equation developed by Badhwar<sup>[3]</sup> were used, respectively. The omnidirectional fluence and unidirectional fluence considering various viewing angles in the analysis period can be determined by repeating the above calculations periodically.

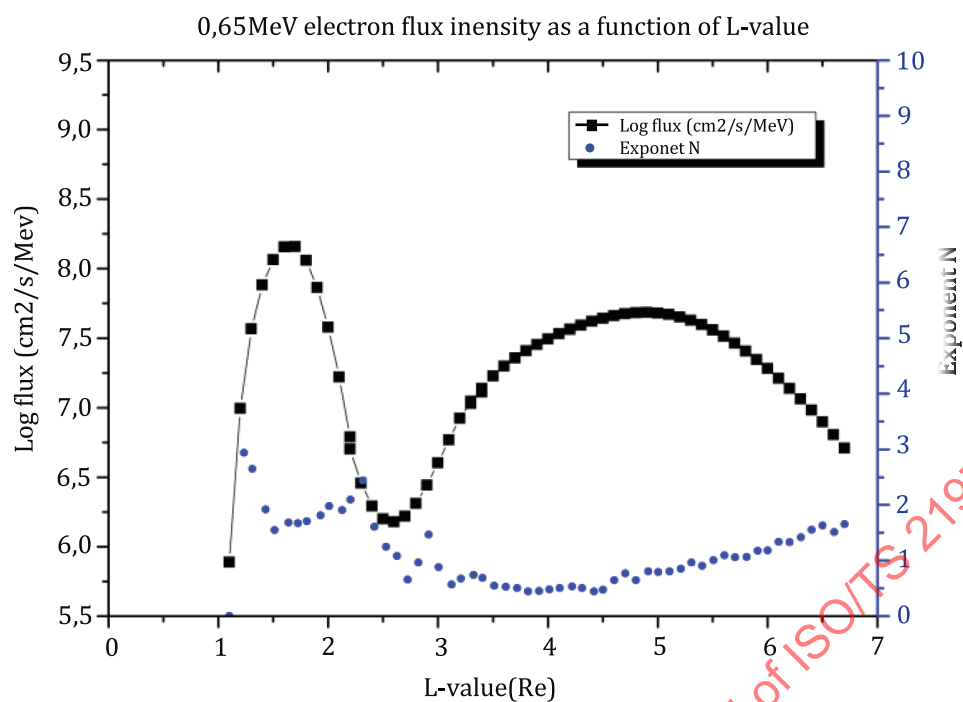
Figure C.5 shows the omnidirectional flux predicted using the developed model for the period during which MDS-1 was in operation. The Ap index, solar wind speed, and F10.7 index were obtained from the OMNIWeb service provided by the Goddard Space Flight Center. Compared with the measured data, the model can reproduce the variation of radiation in the outer belt and the existence of the slot

region reasonably well. [Figure C.6](#) shows the cross-sectional image of the radiation belt for orbit No. 80 under a normal state and orbit No. 175 where flux increases and the value of  $n$  changes. As shown in [Fig. C.6](#), the phenomena are successfully reproduced (i.e., peak of the radiation belt shifts inward and the distribution of  $n$  changes with increasing flux). [Figure C.7](#) shows the program flow for calculating the number of incident particles on the target.



**Figure C.5 — Results for MDS-1 orbit predicted using the dynamic radiation belt model (where energy width of the bin is 0,35 to 0,78 MeV and the mean value is 0,65 MeV)**





(a) 80 orbits (nominal case)